Quasi-Disorder Effects in Topological Superconductors

M. F. Madeira
CeFEMA, Instituto Superior Técnico, Universidade de Lisboa, Av. Rovisco Pais, 1049-001 Lisboa, Portugal
(Dated: May 20, 2022)

We study the effects of quasi-disorder and random disorder in a model of a two dimensional topological superconductor with an applied external magnetic field. The cases of a p-wave superconductor and a noncentrosymmetric superconductor with mixed p- and s-wave pairing and Rashba spin orbit coupling are studied. We first review the topological properties of the clean system. The disordered system is then studied both in real space and in a mixed space. When the applied magnetic field is parallel, we study both edge and bulk quasi-disorder and random disorder and discuss their effects on a real space approach. Also on a real space approach we show that, for a perpendicular magnetic field, the introduction of quasi-disorder leads to the appearance of new topological phases, characterized by an integer value of the Chern number. In a mixed space approach we identify new regimes with the appearance of new Majorana flat bands and also new unidirectional Majorana edge states, as quasi-disorder is introduced. We show the Majorana flat bands have a quantized Berry phase of π and identify this as a topological invariant. Two topological transitions are identified and the values of the critical exponents z and ν are obtained. The fractal nature of the eigenstates is discussed both for Anderson disorder and Aubry-André disorder.

I. INTRODUCTION

The search and study of topological properties of matter has proved fruitful in recent years in research in materials science and condensed matter physics. Superconductors with intrinsic topological properties, in particular, have recently attracted interest due to phenomena associated with surface or edge Majorana modes, which appear from an interplay between topology and bulk-boundary correspondence [1–3].

In this work we will study a model of a two-dimensional topological superconductor with spin triplet p-wave pairing, or mixed p- and s-wave pairings with Rashba spin-orbit coupling, in the presence of a magnetic field which breaks time reversal symmetry. In the presence of s-wave pairing and Rashba spin orbit coupling, the model describes a noncentrosymmetric superconductor. The clean model has been studied and is known to possess diverse topological properties, which depend on the direction of the applied magnetic field with respect to the plane of the superconductor [4, 5]. We are interested in studying the effects of quasi-disorder in these regimes, on topological and localization properties. Besides Aubry-André disorder [6], we will also consider Anderson disorder as a comparison to the effects of quasi-periodicity.

II. MODEL HAMILTONIAN

In momentum space, the BdG Hamiltonian matrix is written as

$$\mathcal{H}(\mathbf{k}) = \begin{pmatrix} \xi(\mathbf{k}) + \mathbf{B}\cdot\boldsymbol{\sigma} & \Delta(\mathbf{k}) \\ \Delta^{\dagger}(\mathbf{k}) & -\xi^{T}(-\mathbf{k}) - \mathbf{B}\cdot\boldsymbol{\sigma}^{*} \end{pmatrix} \qquad (1)$$

in a basis $(\boldsymbol{c}^{\dagger}_{\mathbf{k}}, \boldsymbol{c}_{-\mathbf{k}}) = (c^{\dagger}_{\mathbf{k}\uparrow}, c^{\dagger}_{\mathbf{k}\downarrow}, c_{-\mathbf{k}\uparrow}, c_{-\mathbf{k}\downarrow})$ with $c^{\dagger}_{\mathbf{k}s}$ ($c_{\mathbf{k}s}$) the creation (annihilation) operator for an electron with momentum $\boldsymbol{k} = (k_x, k_y)$ and spin s. In the BdG Hamiltonian, $\xi(\boldsymbol{k}) = \epsilon_{\boldsymbol{k}}\sigma_0 + \mathbf{s}\cdot\boldsymbol{\sigma}$, where $\epsilon_{\mathbf{k}} = [-2t(\cos k_x + \cos k_y) - \mu]\,\sigma_0$ is the kinetic term, with t the nearest-neighbour hopping integral and μ the chemical potential, $\mathbf{s}\cdot\boldsymbol{\sigma} = -\alpha(-\sin k_y, \sin k_x, 0)\cdot\boldsymbol{\sigma} = -\alpha\left[-\sin k_y\sigma_x + \sin k_x\sigma_y\right]$ is the spin-orbit term with $\mathbf{s}$ the spin-orbit vector. The term $\mathbf{B}\cdot\boldsymbol{\sigma}$ describes the Zeeman coupling of the electrons with an external magnetic field $\mathbf{B}$ and $\hat{\Delta}(\mathbf{k}) = [\Delta_s + \mathbf{d}(\mathbf{k})\cdot\sigma]\,(i\sigma_y)$ is the superconducting gap function. The pairing vector is chosen as $\mathbf{d} = d(-\sin k_y, \sin k_x, 0)$. The simultaneous existence of s and p wave terms is possible with a nonzero spin-orbit term, which breaks the parity symmetry.

The case of study is that of a system with periodic boundary conditions along the x direction and open boundary conditions in the y direction, such as in a cylinder geometry. Thus we can also write the Hamiltonian in a mixed space (k_x, y). In this case, for each value of k_x the Hamiltonian matrix has a dimension $(4\times N_y)\times(4\times N_y)$, where N_y is the number of sites in y. It is also of interest to write the Hamiltonian in real space. In this case the Hamiltonian matrix has a dimension $(4\times N)\times(4\times N)$ with $N = N_x \times N_y$ the total number of sites, and N_x, N_y the number of sites in the x and y directions, respectively.

When $\mathbf{B} = 0$, the system respects time-reversal symmetry and particle-hole symmetry and belongs to the DII symmetry class. If $|d| > |\Delta_s|$ the system has a nontrivial $\mathbf{Z}_2$ number, displaying gapless counterpropagating Majorana edge states (MESs). [4, 5]. For $\mathbf{B} \neq 0$ the time-reversal symmetry is broken. The system exhibits different topological properties whether the applied magnetic field is perpendicular or parallel to the plane of the system, as will be now discussed.

III. CLEAN SYSTEM

A. Perpendicular magnetic field

Let us first consider the case in which the external magnetic field is perpendicular to the plane of the system, $\mathbf{B} = (0, 0, B_z)$. We have a gap closing if one of the

equations is satisfied:

$$(-4t-\mu)^2+\Delta_s^2=B_z^2,\quad (4t-\mu)^2+\Delta_s^2=B_z^2,\\ \mu^2+\Delta_s^2=B_z^2 \tag{2}$$

Equations 2 define the boundaries between regions in which the system has different topological properties, characterized by the Chern number. The phase diagram of the system indexed by the Chern number is presented in figure 1 a) for $\Delta_s=0$.

The regimes with a Chern number of zero and $B_z<2$, $|\mu|<4t$ exhibit edge states, besides having $C=0$. This can be explained by one additional topological invariant. It can be defined noting that the Hamiltonian obeys a particle hole symmetry $\mathcal{P}=(\sigma_x\otimes\sigma_0)$ with

$$\mathcal{P}\mathcal{H}(\mathbf{k})\mathcal{P}^\dagger=-\mathcal{H}^*(-\mathbf{k}). \tag{3}$$

For the values $k_y=0$ and $k_y=\pi$, the Hamiltonian obeys $\mathcal{H}^*(-\mathbf{k})=\mathcal{H}(\mathbf{k})$ and thus anticommutes with $\mathcal{P}$, $\{\mathcal{H}(\mathbf{k}),\mathcal{P}\}=0$. Therefore the basis which diagonalizes $\mathcal{P}$ anti-diagonalizes the Hamiltonian. A winding number $I(k_y)$ can then be defined as [7]

$$I(k_y)=\frac{1}{4\pi i}\int_{-\pi}^{\pi}dk_x\,\mathrm{tr}\left[q^{-1}(k_x)\partial_{k_x}q(k_x)-\right.\\ \left.q^{\dagger-1}(k_x)\partial_{k_x}q^\dagger(k_x)\right],\quad k_y=0,\pi, \tag{4}$$

where $q(k_x)$ is the anti-diagonal block of the Hamiltonian written in the new basis. The values of $I(0)$ and $I(\pi)$ inside each phase are represented in figure 1 b).

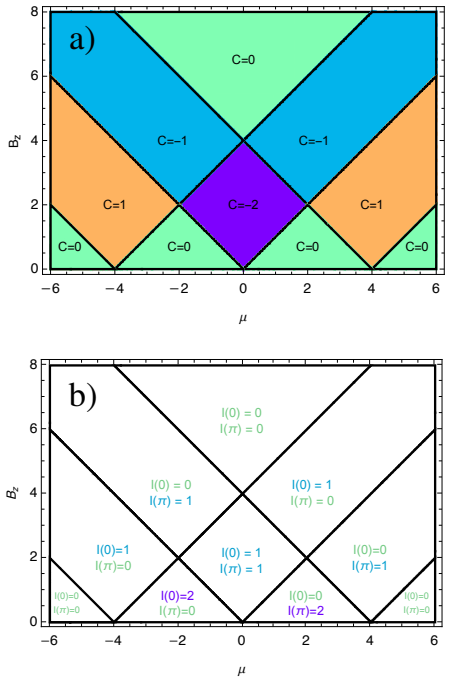

Figure 1. Phase diagram for a) the Chern number and b) the winding numbers $I(k_y=0,\pi)$ as a function of μ and B_z, with $t=1$ and $\Delta_s=0$ and for $d>0$.

The invariant $I(k_y)$ loses its meaning if any magnetic field B_y is applied. However, we found that this is not true for the Chern number. Figure 2 shows the phase diagram for the Chern number as a function of B_z and B_y at three different values of μ. In this case the Chern number depends only on the value of $\sqrt{B_y^2+B_z^2}$. Also note that the diagram only concerns values of $B_z>0$, excluding the points where $B_z=0$ and $B_y\neq 0$.

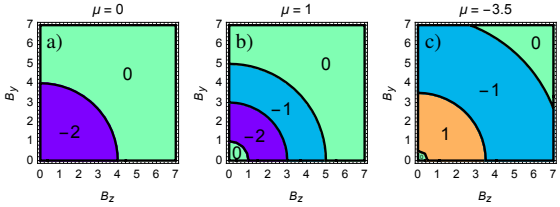

Figure 2. Phase diagram for $(B_z>0, B_y)$ for the Chern number obtained numerically at a) $\mu=0$, b) $\mu=1$ and c) $\mu=-3.5$ for $\Delta_s=0$.

B. Parallel magnetic field

Now let us consider the case in which the external magnetic field applied is parallel to the system, $\mathbf{B}=(B_x,B_y,0)$. Taking the s-wave term Δ_s and the spin-orbit term α to be zero, the eigenvalues of the Hamiltonian are given by

$$E(\mathbf{k})=\pm\sqrt{z_1\pm 2\sqrt{z_2}}. \tag{5}$$

with

$$z_1=\mathbf{d}\cdot\mathbf{d}+\epsilon_{\mathbf{k}}^2+\mathbf{B}\cdot\mathbf{B},\quad z_2=\epsilon_{\mathbf{k}}^2(\mathbf{B}\cdot\mathbf{B})+(\mathbf{B}\cdot\mathbf{d})^2. \tag{6}$$

The gap closing points are solutions of the equation $z_1=2z_2$, which is equivalent to the two equations being simultaneously satisfied:

$$\mathbf{d}\cdot\mathbf{d}+\epsilon_{\mathbf{k}}^2=\mathbf{B}\cdot\mathbf{B},\quad (\mathbf{B}\cdot\mathbf{B})(\mathbf{d}\cdot\mathbf{d})=(\mathbf{B}\cdot\mathbf{d})^2. \tag{7}$$

Equations 7 simplify if we consider the magnetic field aligned with one of the axes. Let us take the magnetic field aligned with the $y-$direction, $\mathbf{B}=(0,B_y,0)$. In this case, the second equation simplifies to $\sin k_y=0$ which implies the bulk gap will close at $k_{y,0}=n\pi, n\in\mathbb{Z}$, provided there are values of k_x that satisfy the equations

$$d^2\sin^2 k_x+(-2t(\cos k_x\pm 1)-\mu)^2=B_y^2. \tag{8}$$

When the p-wave superconductor is in a gapless phase, and for a certain range of magnetic field, Majorana flat bands (MFBs) will appear in the system. This will be discussed next. Also, when finite spin-orbit α or s-wave pairing Δ_s terms are introduced, the flat bands will acquire a slope and give origin to unidirectional Majorana edge states (MESs).

1. Flat bands: winding number and Berry phase quantization

Let us consider a generic parallel magnetic field of the form $\mathbf{B} = (B_x, B_y, 0)$. In this case the system no longer respects time-reversal symmetry. We can, however, take k_x as a fixed parameter of the Hamiltonian and find a set of symmetries that are only satisfied in the y-direction. It is found that the Hamiltonian respects the symmetries

$$\begin{aligned} \mathcal{T}_{k_y}^{-1}\mathcal{H}(k_x,k_y)\mathcal{T}_{k_y} &= \mathcal{H}(k_x,-k_y), \\ \mathcal{P}_{k_y}^{-1}\mathcal{H}(k_x,k_y)\mathcal{P}_{k_y} &= -\mathcal{H}(k_x,-k_y) \end{aligned} \tag{9}$$

where $\mathcal{T}_{k_y} = (\sigma_z \otimes \sigma_z)K$ and $\mathcal{P}_{k_y} = (\sigma_y \otimes \sigma_y)K$ are, respectively, defined as a "time-reversal-like" symmetry and a "particle-hole-like" symmetry [5] with $\mathcal{T}_{k_y}^2 = \mathcal{P}_{k_y}^2 = 1$. From these we can define a third chiral-like symmetry $\mathcal{S}_{k_y} = \mathcal{T}_{k_y}\mathcal{P}_{k_y}$:

$$\mathcal{S}_{k_y}^{-1}\mathcal{H}(k_x,k_y)\mathcal{S}_{k_y} = -\mathcal{H}(k_x,k_y). \tag{10}$$

Since we have that $\mathcal{T}_{k_y}^2 = \mathcal{P}_{k_y}^2 = 1$, the Hamiltonian belongs to the BDI symmetry class and, since the problem is effectively reduced to one dimension, the system can be characterized by an integer topological invariant. We can then write the Hamiltonian in the basis where $\mathcal{S}_{k_y}$ is diagonal, in which the Hamiltonian takes an anti-diagonal form. From here it is possible to obtain the winding number $\mathcal{W}$. It can be shown [5] that the winding number is calculated as

$$\mathcal{W} = \frac{i}{\pi}\left[\log\left(\frac{sgn(\mathcal{M}(k_y=0))}{sgn(\mathcal{M}(k_y=\pi))}\right)\right] \tag{11}$$

with

$$\begin{aligned} &\mathcal{M}(k_x,k_y) = \\ &\left[\mu + 2t\left(\cos k_x + \cos k_y\right)\right]^2 + d^2\sin^2 k_x - B_y^2 + B_x^2. \end{aligned} \tag{12}$$

In the regimes with $|\mathcal{W}| = 1$ the system has a topological nature and Majorana flat bands appear. These are protected by the chiral symmetry as defined in equation 10. We have found that in the regimes with $|\mathcal{W}| = 1$, the Berry phase is also quantized to a value of π.

2. Domain of flatband existence

From equation 11 it is found that $|\mathcal{W}| = 1$ in the regimes where $\mathcal{M}(k_x, k_y = 0)$ and $\mathcal{M}(k_x, k_y = \pi)$ have opposite signs, $\mathcal{M}(k_x, k_y = 0)\,\mathcal{M}(k_x, k_y = \pi) < 0$. This allows us to derive the regions in which the superconductor possesses flat band, which can be summarized in (with $\tilde{B}^2 = B_y^2 - B_x^2$ and $|B_y| > |B_x|$):

- (1) $\mu \geq 2t$

$$\mathcal{D}_+ > \tilde{B}^2 > \mathcal{D}_- \tag{13}$$

- (2) $\mu \leq -2t$

$$\mathcal{D}_- > \tilde{B}^2 > \mathcal{D}_+ \tag{14}$$

- (3) $-2t < \mu < 2t$

$$(\mathcal{D}_+ > \tilde{B}^2 > \mathcal{D}_-) \vee (\mathcal{D}_- > \tilde{B}^2 > \mathcal{D}_+) \tag{15}$$

with

$$\mathcal{D}_\pm = \left[\mu + 2t\left(\cos k_x \pm 1\right)\right]^2 + d^2\sin^2 k_x. \tag{16}$$

Equations 13, 14 and 15 define the regions where the superconductor is in a nontrivial regime with $|\mathcal{W}| = 1$ (which coincide with the regions where the bulk is gapless).

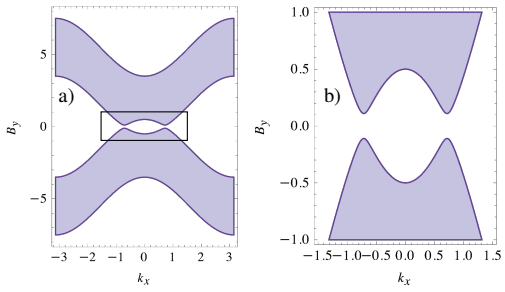

Figure 3. a) Domain of existence of Majorana flat bands (shaded region) for B_y vs. k_x for the parameters $t = 1$, $d = t/6$, $\mu = -3.5$. b) Closeup of a) in the region $B_y \in [-1, 1]$ and $k_x \in [-1.5, 1.5]$.

IV. QUASI-DISORDER AND ANDERSON DISORDER EFFECTS IN REAL SPACE

We now consider the case in which disorder is added to the model. A system with $41 \times 41 = 1681$ sites (with $N_x = N_y$) is studied, and we consider periodic boundary conditions along x and open boundary conditions along y. We add a new term to the real space Hamiltonian with a disorder term $\Lambda(\mathbf{r})$, and we consider disorder of two types: Anderson disorder, where the disorder is random at each site and the random values vary between an interval,

$$\Lambda(\mathbf{r}) \in [-\lambda, \lambda], \tag{17}$$

and Aubry-André disorder, where the disorder term is a quasi-periodic potential of the form:

$$\Lambda(\mathbf{r}) = \lambda\cos(2\pi\alpha f(\mathbf{r}) + \phi) \tag{18}$$

with $f(\mathbf{r})$ a function of the lattice sites, $\alpha = \frac{\sqrt{5}-1}{2}$ the inverse golden ratio, and ϕ a phase between 0 and 2π. To quantify the effects of disorder we use the inverse participation ratio, IPR, defined as

$$\mathcal{IPR}_m = \sum_i |\psi_i^m|^4. \tag{19}$$

For perfectly localized states we have that $\mathcal{IPR}_m \sim 1$ and for delocalized states $\mathcal{IPR}_m \sim 1/N$.

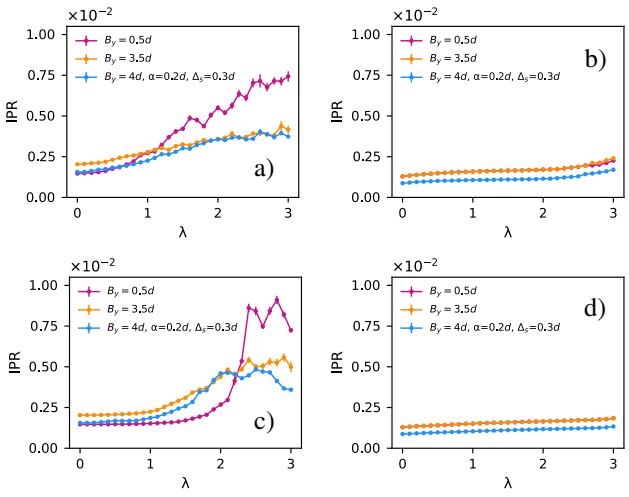

Figure 4. First column: IPR averaged over the lowest 10 positive energy states and highest 10 negative energy states, vs. a) Anderson edge disorder strength or c) Aubry-André edge disorder strength. Second column: IPR averaged over the remaining states vs. b) Anderson edge disorder strength or b) Aubry-André edge disorder strength.

A. Edge disorder with a parallel magnetic field

We first consider Anderson disorder and Aubry-André disorder, localized at $y = 0$ and $y = N_y$ and varying along the x direction. Here we limit ourselves to the cases where the magnetic field $\mathbf{B}$ is aligned in the y direction and consider either p-wave pairing symmetry or combined s and p-wave pairings when the spin-orbit term is finite. We take the fixed values $t = 1, d = t/6, \mu = 3d - 4t$, and consider three cases in detail: the case in which a magnetic field $B_y = 0.5d$ is added (phase with a gapped bulk but gapless edge states); an added magnetic field of $B_y = 3.5d$ (phase with a gapless bulk and in in the MFB regime); and the noncentrosymmetric case with $B_y = 4d$ and added $s-$wave pairing and spin-orbit terms, $\Delta_s = 0.3d$ and $\alpha = 0.2d$ (phase with a gapless bulk and MESs).

In figure 4 we show the IPR for the lower energy states in a) and c), for Anderson edge disorder and Aubry-André disorder, respectively, and the averaged IPR of the remaining bulk states, in b) for Anderson edge disorder and in d) for Aubry-André edge disorder. From b) and d) we see that the bulk states are almost unaffected by the introduced edge disorder. There is only a slight increase in the IPR, which is larger in the Anderson disorder case. The localization happens mostly on lower energy states, which is seen in figures a) and c). In a) we see that there is a continuous increase of the IPR. In c) we see a different behaviour - the lowest energy states seem mostly unaffected (with constant IPR) until a certain threshold value of disorder. Also, in both a) and c), for the system with $B_y = 0.5d$ the low energy states become more localized with increased disorder in relation to the states in the MFB and MESs regimes, which appear to be more robust at higher values of disorder.

In figure 5 we show some edge states at different values of a) Anderson edge disorder and b) Aubry-André edge disorder. In the Anderson disorder case in a), for $\lambda = 0.5$ we see that the state already lost its periodic modulation along the edges. For $\lambda = 1.0$ we see an intermediate state, and for $\lambda = 2.7$ the state is already mostly localized on the edge at $y = 40$. We found that initially the edge states follow a similar behaviour in both edges. At higher values of disorder the states become significantly more localized in only one edge (which one depends on the random disorder configuration). For Aubry-André edge disorder, at $\lambda = 0.5$ the state as a whole is mostly unaffected, and the effect of the quasi-periodic disorder is seen on the edge layers. In b), for a higher value of disorder of $\lambda = 1.0$ the state becomes more localized, both along the edges and along the y direction. In c) for $\lambda = 2.7$ the state localizes at several values of x along the edges, and also appears to localize along y. In this case the same value of ϕ was considered at both edges, and, accordingly, the behaviour is mirrored, with the states staying localized at both edges for high disorder values.

For both Anderson edge disorder and Aubry-André edge disorder, we have also seen that the bulk layers are also affected by the edge disorder, and that the contribution of the wavefunctions can increase for some of the subsequent y layers.

B. Bulk disorder with a parallel magnetic field

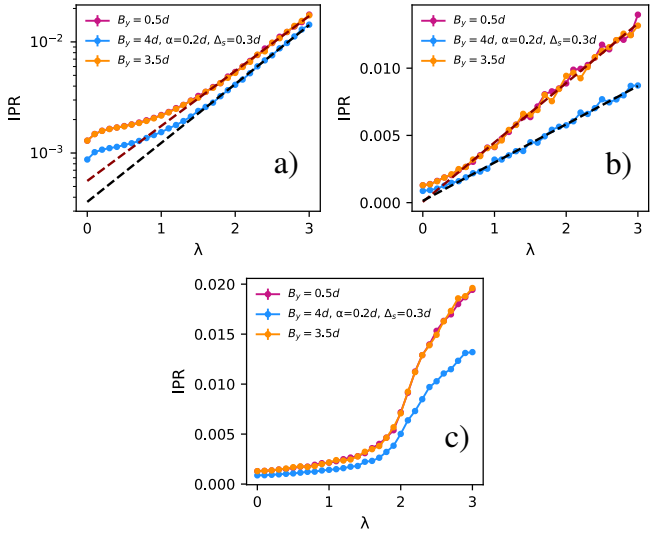

Figure 6. Average IPR of the whole system for a) Anderson disorder, b) Anderson disorder with x periodicity, c) Aubry-André disorder. In a) fits are done to functions of the form $y = C_1 \exp C_2 x$ in the range $\lambda \in [1.5, 3]$. In b) fits are done to functions of the form $y = C_1 x + C_2$ in the range $\lambda \in [0.5, 3]$.

We now consider bulk disorder of three types: Anderson disorder; Anderson disorder uniform in x; Aubry-André disorder modulated in y and uniform in x. We study the same parameter cases as in subsection IV A.

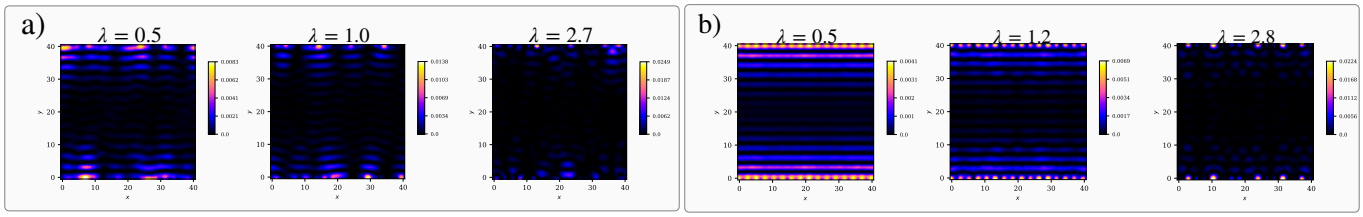

Figure 5. Disordered edge states for $t = 1$, $d = t/6$, $\mu = -3.5$, $B_y = 4d$, $\alpha = 0.2d$ and $\Delta_s = 0.3d$, subject to a) Anderson edge disorder and b) Aubry-André edge disorder. In a) the wavefunctions have energies $E = 8 \times 10^{-4}$ (left), $E = 8 \times 10^{-4}$ (middle) and $E = 9 \times 10^{-4}$ (right). In b) the wavefunctions have energies $E = 8 \times 10^{-4}$ (left), $E = 8 \times 10^{-4}$ (middle) and $E = 9 \times 10^{-4}$ (right).

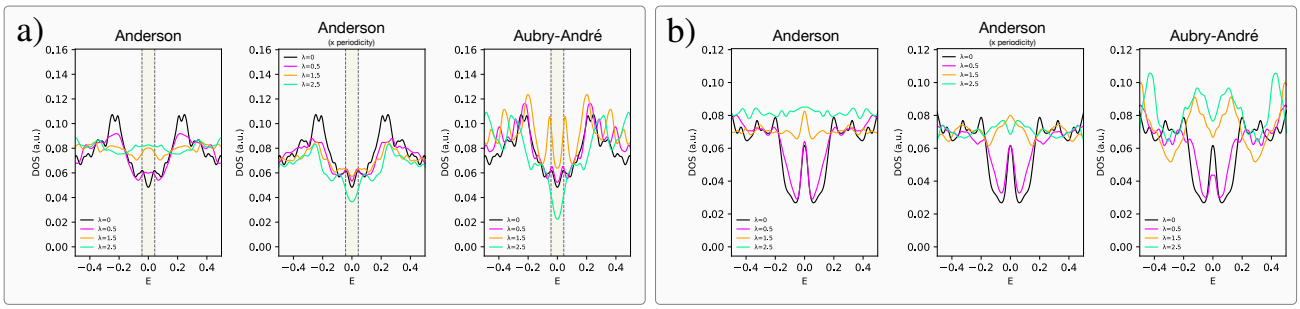

Figure 7. Total density of states of the system, for the energy range $E \in [-0.5, 0.5]$, obtained with the Recursive Green's Function method for several values of λ. Obtained for Anderson disorder, Anderson disorder uniform in x and Aubry-André disorder, and for the parameter values a) $B_y = 0.5d$, b) $B_y = 4d, \alpha = 0.2d, \Delta_s = 0.3d$. The DOS is obtained for an average of 20 initial random states and disorder configurations.

The values of the averaged IPR are shown respectively in a), b) and c). For Anderson disorder, the IPR follows an exponential behaviour for $\lambda > 1.5$. We show of a function of the type $y = C_1 \exp C_2 x$ with C_1, C_2 constants, for the interval $[1.5, 3.0]$. In b), the IPR follows a nearly linear behaviour for $\lambda > 0.5$ and we show a fit to function of the form $y = C_1 x + C_2$ which is done to the interval $[0.5, 3.0]$. In c), we see a threshold behaviour around $\lambda = 2.0$ and with two different regimes: in the first there is a slow increase of the IPR, and then it greatly increases. For $\lambda < 2.0$ we observed that some bulk wavefunctions acquire a critical-like behaviour along the y direction.

In figure 7 we show the DOS for $E \in [-0.5, 0.5]$, for a) $B_y = 0.5d$ and for b) the noncentrosymmetric case with $B_y = 4d, \alpha = 0.2d, \Delta_s = 0.3d$. In a) the gap of the clean system, which is located around $E \in [-0.044, 0.044]$, is highlighted. The results are presented for several values of λ and for all the disorder cases considered. For Anderson disorder, we see that the increase of λ leads to a monotonic increase of the DOS at zero energy in both cases a) and b). With Anderson disorder uniform in x, in a) there is first an increase and then a decrease of the DOS at zero energy (in relation to the clean system). In b) the DOS around zero energy increases and then slightly decreases (as seen for $\lambda = 2.5$). The right panels concern the case of Aubry-André disorder. In b) the DOS around zero energy first decreases and then increases with disorder. In a), we see first that the DOS increases slightly around zero energy. For $\lambda = 1.5$ there is a further increase and for $\lambda = 2.5$ the value decreases, with the system being actually gapped (this is not seen in the figure since the curve is smoothed for visualization purposes).

C. Quasi-disorder induced topology with a perpendicular magnetic field: Chern number

We now want to investigate the effects of quasi-disorder on the system when in the presence of an applied magnetic field in the perpendicular direction, $\mathbf{B} = (0, 0, B_z)$. To classify the topological nature of the system the Chern number is calculated in real space [8]. Figure 8 shows six phase diagrams for three different values of μ and d (with $t = 1$ in all cases) obtained for a system with size 20×20, for Anderson disorder (first row) and Aubry-André disorder (second row), both uniform in the x direction.

When Anderson disorder is introduced (first row) in the system the topological regimes are destroyed as the disorder strength is increased. We see that some values of B_z are more robust than others, particularly the values which are halfway inside the topological phases of the clean system. Unexpectedly, at low values of magnetic field, we see some small traces of topology appear as disorder is increased for values of B_z where the Chern number was previously zero.

In the case of Aubry-André disorder (second row) we obtain phase diagrams with reentrant topological regions. Different types of transitions are illustrated. In the diagram for $\mu = 0$ and $d = 0.6$ (left) we see the appearance

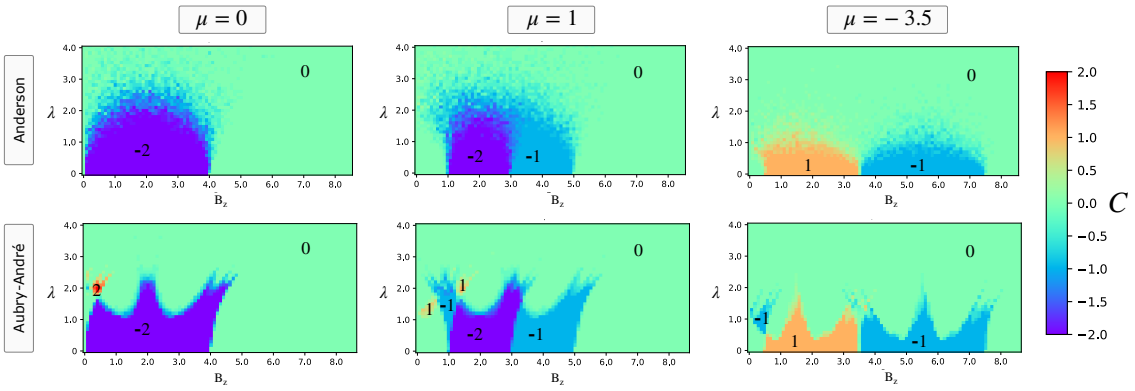

Figure 8. Phase diagrams of a system with 20x20 sites indexed by the Chern number C, for several values of disorder strength λ and perpendicular magnetic field B_z, obtained for the average over 10 disorder configurations. The first row concerns the case of Anderson disorder and the second row concerns Aubry-André disorder. The values of the parameters are $t = 1$, $d = 0.6$ and $\mu = 0$ (left), $d = 0.6$ and $\mu = 1$ (middle), $d = 1/6$ and $\mu = 3d - 4t = -3.5$ (right).

of a small region characterized by $C = 2$. For $\mu = 1$ and $d = 0.6$ (middle), we see the appearance of two small regions with $C = 1$, that however seem to be averaged out. In the approximate range of $B_z \in [0.3, 1.3]$ there is also a reentrant topological region with $C = -1$. Inside this range, for $B_z < 1$, we have topological transitions $C = 0 \to C = -1$ with increasing λ. For $B_z \in [1, 1.3]$, there is a transition $C = -2 \to C = -1$. At $\mu = -3.5$, $d = 1/6$ (right) a new region with $C = -1$ emerges for $B_z \in [0.1, 0.9]$. Inside this range, for $B_z < 0.5$ a transition $C = 0 \to C = -1$ happens with increasing λ. For $B_z \geq 0.5$ there is a previous transition from $C = 1$ to $C = 0$. Transitions from $C = 0$ to a finite value of C also happen at higher values of the magnetic field. This is evident in the case of $\mu = 0$ for $B_z > 4$ and in the case $\mu = 1$ for $B_z > 5$. For a small region of B_z, with the increase of λ we see a reentrant topological phase in a new region. Also, we note that the topological phases show an interesting response to the increase of quasi-disorder, with a clear difference in robustness for different values of B_z as quasi-disorder is increased.

We note that the induced topological regions at low magnetic field come from phases with $C = 0$ that however were not trivial at $\lambda = 0$ due to a finite value of $I(k_y)$ (except in the case of $\mu = 0$). This could possibly explain some of the topological transitions at small values of B_z as quasi-disorder is introduced, in regimes in which the Chern number was previously zero.

To see how the different critical values of quasi-periodic disorder λ scale with the system size, three transitions at fixed values of B_z and μ were considered. The results are presented in figure 9 for the system sizes 20×20, 30×30 and 41×41. The results show that within the considered system size range, the critical values show little variation, thus suggesting that the obtained phase diagrams in 10 should apply to larger systems.

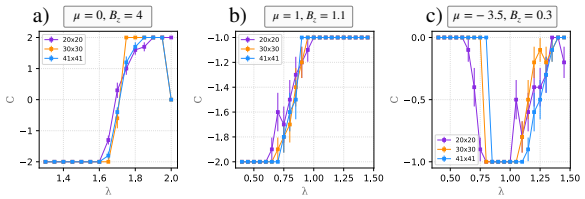

Figure 9. Values of the Chern number C vs. disorder strength λ for the system sizes 20×20, 30×30 and 41×41 and for a) $t = 1$, $\mu = 0$, $d = 0.6$, $B_z = 0.4$, b) $\mu = 1$, $d = 0.6$, $B_z = 1.1$, c) $\mu = -3.5$, $d = 1/6$, $B_z = 0.3$. The results were averaged over 10 disorder configurations (10 random values of ϕ in the quasi-periodic potential).

V. QUASI-DISORDER AND ANDERSON DISORDER EFFECTS IN MIXED (k_x, y) SPACE

In a mixed (k_x, y) space, $\Lambda(y)$ is the disorder term which can be of the form of either Equation 17 (Anderson disorder) or Equation 18 (Aubry-André disorder). The disorder potential can only vary in the y direction and is the same for all k_x.

A. Energy spectra evolution and density of states

In figure 10 we present the energy spectra for some values of Anderson disorder (first row) and Aubry-André disorder (second row), for $t = 1$, $d = t/6$, $\mu = -3.5$, and $B_y = 0.5d$ in a) and c) and $B_y = 4d$, $\alpha = 0.2d$, $\Delta_s = 0.3d$ in b) and d). We also show the DOS, obtained from exact diagonalization of the system, for several values of λ.

First we look at the Anderson disorder case, panels a) and b). In a) the system has gapless edge states and a bulk gap. We find that, as disorder is increased, the edge states lose their structure and the bulk gap is closed. Accordingly, there is an increase in the DOS at zero energy. In cases where the bulk is already gapless and Majorana flat bands are present in the clean system (not shown

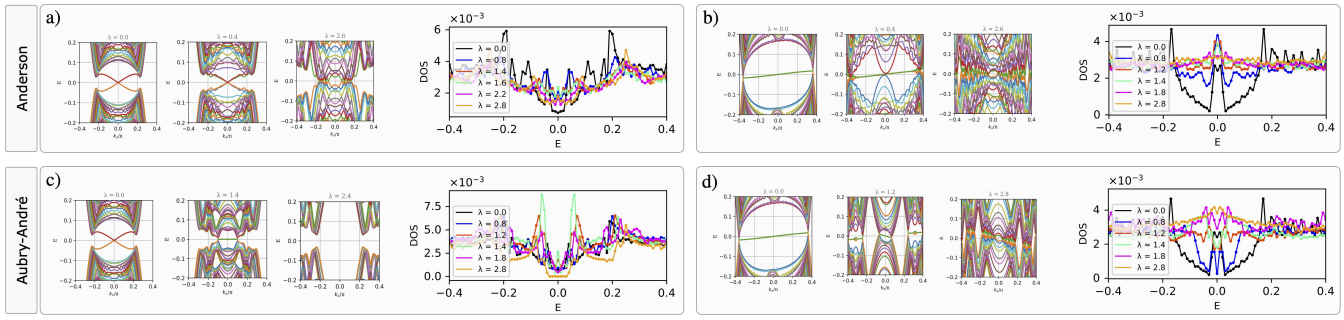

Figure 10. Top: evolution of energy spectra and density of states for Anderson disorder for a) $B_y = 0.5d$, and b) $B_y = 4d$, $\alpha = 0.2d$, $\Delta_s = 0.3d$. Bottom: evolution of energy spectra and density of states for Aubry-André disorder, for c) $B_y = 0.5d$ and d) $B_y = 4d$, $\alpha = 0.2d$, $\Delta_s = 0.3d$.

here) we found that the bulk remains gapless, and that the Majorana flat bands are not lifted to finite energies. In b) the system describes a noncentrosymmetric superconductor with mixed s and p-wave pairings. The system is in the regime where unidirectional MESs appear. These are robust to small values of disorder strength, but as disorder increases the structure of the band is lost, and bulk states collapse to lower energy values.

Panels c) and d) portrait the same parameter values as a) and b) respectively but with added Aubry-André disorder. In c), around $\lambda = 1.2$ the bulk gap is closed and a new flat band appears, which leads to an increase of the DOS at zero energy. The flat band then splits in two and disappears as a gap opens in the system for around $\lambda = 1.8$. This reopening of the bulk gap contrasts with what is found for Anderson disorder in a), where the bulk remains gapless as disorder is increased. When quasi-disorder is introduced in gapless regimes, we found that it will also introduce new regions with flat bands.

We also found that quasi-disorder induces new unidirectional edge states in the noncentrosymmetric superconductor. In d), when a certain value of disorder is reached, "flipped" unidirectional states appear in the system. This can be seen for the value of $\lambda = 1.2$, as a band with negative slope appears for values of k_x around $k_x = 0$. At this disorder value there is a coexistence of unidirectional "flipped" left-moving edge modes (with negative slope) around $k_x = 0$ and right-moving edge modes (with positive slope) for higher (absolute) values of k_x. A backflow current that balances the current on the edges is created on the bulk: extra right or left moving modes will appear depending on the net current on the edges. For $\lambda > 1.2$ the structure of the right-moving unidirectional states starts to be lost.

B. Quasi-disorder induced Majorana Flat Bands

We want to investigate if the quasi-disorder induced flat bands have a topological nature. Since the Berry phase was found to be quantized to a value of π in the clean system in the region of MFBs, we calculate it here for the disordered case. The Berry phase is obtained in real space using twisted boundary conditions. Considering a twisted boundary phase θ_y we have:

$$\gamma = i \int_0^{2\pi} \langle \Psi(\theta_y) \mid \frac{\partial}{\partial \theta_y} \Psi(\theta_y) \rangle \tag{20}$$

where Ψ denotes the ground-state many body wavefunction, which can be represented by an $M \times N$ matrix $\mathbf{\Psi}^{\theta_y}$ where N is the number of sites in y and M is the number of occupied states. The twist variable is discretized into L points between 0 and 2π. A link variable can then be defined as $U(\theta_{y,n}) = \det\left[\mathbf{\Psi}^{\dagger}{}_{\theta_{y,n}} \mathbf{\Psi}_{\theta_{y,n+1}}\right]$, and the Berry phase is obtained as

$$\gamma = -\mathrm{i} \sum_{n=1}^{L} \log U(\theta_{y,n}). \tag{21}$$

We obtained the result that the quasi-disorder induced MFBs have a quantized Berry phase of π, as it can be seen in figure 11.

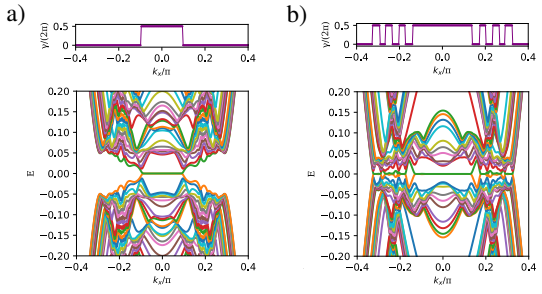

Figure 11. Energy spectrum and Berry phase normalized by 2π, as a function of k_x. The values of the parameters are $t = 1$, $d = t/6$, $\mu = 3d - 4t$ and a) $B_y = 0.5d$, $\lambda = 1.4$ b) $B_y = d$, $\lambda = 1.6$.

To quantify the induced bands at zero energy and study the transition to a π-quantized Berry phase, we use the concept of Majorana pair density [9]:

$$\rho_\gamma = \frac{N_\gamma}{N_k}, \tag{22}$$

where N_k is the number of discrete points of k_x taken inside the interval $[-\pi, \pi]$ and N_γ is the number of such points which support MFBs at the edges. A transition from $\rho_\gamma = 0$ to $\rho_\gamma \neq 0$ signals a transition from a trivial to a topological regime (π-quantized Berry phase). Figure 12 a) shows the evolution of ρ_γ as a function of the quasi-disorder strength λ for the case $t = 1$, $d = t/6$, $\mu = 3d - 4t$ and $B_y = 0.5d$ for the range $\lambda \in [1, 2]$. A transition $\rho_\gamma = 0 \to \rho_\gamma \neq 0$ occurs between $\lambda = 1.22$ and $\lambda = 1.23$ at a certain critical value $\lambda_{C,1}$. A second transition occurs between 1.79 and 1.8, at a critical value $\lambda_{C,2}$, where ρ_γ becomes zero. In Figure 12 b) the normalized density of states at zero energy $\rho(E = 0)$ is shown, for the same parameters and system size as in Figure 12 a), along with the corresponding contribution for the zero energy DOS which comes from the MFB, $\rho(E = 0)_\gamma$. Inside the topological phase we can see that the finite value of $\rho(E = 0)$ observed for the system with OBC comes almost entirely from the presence of flat bands.

Table I shows the values of $\lambda_{C,1}$ and $\lambda_{C,2}$ for several system sizes. It is found that the values of the critical points show little variation with the system size.

N_y	$\lambda_{C,1}$	$\lambda_{C,2}$
76	1.225 ± 0.005	1.800 ± 0.005
100	1.215 ± 0.005	1.775 ± 0.005
175	1.230 ± 0.005	1.805 ± 0.005
200	1.220 ± 0.005	1.800 ± 0.005
400	1.230 ± 0.005	1.805 ± 0.005
800	1.225 ± 0.005	1.805 ± 0.005

Table I. Values of the critical exponents $\lambda_{C,1}$ and $\lambda_{C,2}$ for the system sizes $\{76, 100, 175, 200, 400, 800\}$.

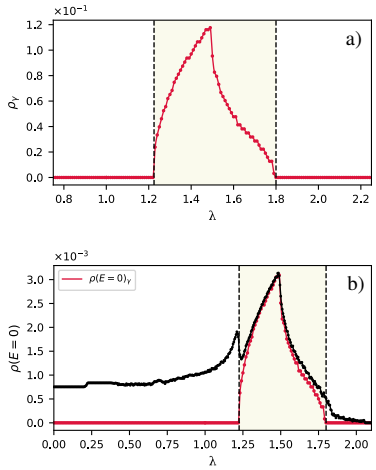

Figure 12. a) Values of ρ_γ for the case $t = 1$, $d = t/6$, $\mu = 3d-4t$ and $B_y = 0.5d$ vs. quasi-disorder strength λ. Obtained for a system with 76 sites in y. b) Value of the DOS at $E = 0$ for the same parameter values as in a), vs. quasi-disorder strength λ, and the contribution for $\rho(E = 0)$ which comes from the Majorana flat bands in the corresponding regime.

C. Scaling of the density of states: critical exponents

Around a critical point, the density of states $\rho(E)$ follows [10]

$$\rho(E) = \delta^{(d-z)\nu} f(|E|\delta^{-z\nu}), \tag{23}$$

with d the dimension of the system, $\delta = \frac{|\lambda - \lambda_C|}{\lambda_C}$ the normalized distance to the critical point λ_C, and f a scaling function. Right at the critical point, when $\delta = 0$, the DOS behaves as

$$\rho(E) \sim |E|^{\frac{d}{z}-1}. \tag{24}$$

From the behaviour of the density of states near the phase transition and using equations 23 and 24 it is possible to obtain the values of the critical exponents numerically.

We first studied a transition in the clean case, in a system with $N_y = 400$ sites in y. At the usual values $t = 1$, $d = t/6$, $\mu = -3.5$, there is a transition from a trivial to a topological regime at a critical value of the magnetic field $B_{y,C} \approx 0.1097$. From a numerical analysis in which we obtained the DOS at the critical point and close to the critical point for $B_y > B_{y,C}$ (gapless phase), we obtained the values $z = 1.08 \pm 0.07$ and $\nu = 0.95 \pm 0.05$. The values of z and ν were also obtained analytically for the same transition in the clean case, and we obtained the values $z = 1$ and $\nu = 1$. Thus the numerical and analytical results are in good agreement.

We now study a system with $N_y = 800$ sites and consider the obtained critical values $\lambda_{C,1} = 1.225$ and $\lambda_{C,2} = 1.805$ as shown in table I for this system size. A fit of the form of equation 24 for the density of states at the critical points, done in the interval $\mathrm{E} \in [0.005, 0.025]$, gives the values of the critical exponents $z = 1.27 \pm 0.04$ for the first transition and $z = 1.23 \pm 0.03$ for the second transition. To determine the value of ν we take values of λ inside the topological (gapless) phase, $\lambda > 1.225$ and $\lambda < 1.805$, and obtain the density of states close to zero energy. For small values of δ and close to zero energy a collapse of the scaled values of the density of states according to equation 23 is expected.

In figure 13 we show the results for scaled the density of states for: a) values close to the first transition at $\lambda = 1.225$, and b) values close to the second transition at $\lambda = 1.805$. The density of states shows a collapse for a) $z = 1.27$ and $\nu = 0.95$ and b) $z = 1.23$ and $\nu = 1.00$. These results deviate from the known universality classes, thus suggesting that the transitions belong to a novel universality class.

D. Fractal analysis

The emergence of multifractality is characterized by fluctuations of eigenstates. These fluctuactions are manifested in the generalized inverse participation ratio, defined as

$$\mathcal{IPR}_m(q) = \sum_i |\psi_i^m|^{2q}, \tag{25}$$

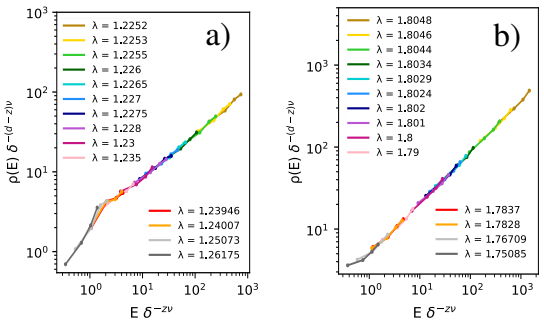

Figure 13. Density of states for $E \in [0.005, 0.025]$ and several values of λ close to the critical values, a) $\lambda_{C,1} = 1.225$ and b) $\lambda_{C,2} = 1.805$, scaled according to Equation 23 for a) $z = 1.27$ and $\nu = 0.95$ and b) $z = 1.23$ and $\nu = 1.00$.

which, at criticality, behaves as [11]

$$\mathcal{IPR}(q) \sim L^{\tau(q)} \tag{26}$$

where L is the system size and the exponent $\tau(q)$ is defined in terms of a generalized dimension $D(q)$ as $\tau(q) = D(q)(q-1)$. In a metallic phase, $D(q) = d$ and for an insulating phase $D(q) = 0$. Wavefunction multifractality is characterized by a q dependent value of $D(q)$, and the cases of a constant $D(q)$ are single fractals [12].

Here k_x is taken at a fixed values, such that system is reduced to an effective one dimension. The IPR as a function of q is calculated and averaged within the energy range $E \in [0.05, 1]$. We fix the parameters $t = 1$, $d = t/6$, $\mu = 3d - 4t$ and $B_y = 0.5d$ and consider both the cases of Aubry-André disorder and Anderson disorder.

The following values of L are considered, to which a fit of an equation of the form of 26 is done: $L_1 = \{75, 100, 150, 175, 200, 255, 275, 400, 475, 600, 675, 800\}$. We also consider the intervals L_2, L_3 and L_4, which are subintervals of L_1 starting at 150, 200 and 275, respectively, to study the behaviour of $\tau(q)$ as L tends to infinity. The obtained results are presented in figure 14.

1. *Anderson disorder*

Figure 14 a) shows the values of $\tau(q)$ for $k_x = 0.02\pi$ and $k_x = 0.2\pi$, for several values of λ and considering the system size interval L_1. For $\lambda = 0$, $\tau(q)$ closely follows the line $\tau(q) = (q-1)$, indicating that $D(q)$ is equal to 1. For higher values of disorder, $\tau(q)$ approaches the line $\tau(q) = 0$, where $D(q) = 0$, suggesting the states are localized and possess a single-fractal nature. For other values of disorder strength $\tau(q)$ does not follow a behaviour characteristic either of $D(q) = 1$ or $D(q) = 0$. It is necessary to evaluate $\tau(q)$ as the system size tends to infinity. In b) several values of $\tau(q)$ are presented, for different values of λ, obtained with fits of the IPR for the size intervals L_1, L_2, L_3 and L_4. For $\lambda = 0$ the values of $\tau(q)$ follow the values of $q-1$ for any interval of L. On the other hand, for finite values of disorder strength, $\tau(q)$ tends to higher values if $q < 1$ and for lower values if $q > 1$ as the system size is increased, which is consistent with a single-fractal behaviour.

2. *Aubry-André disorder*

Figure 14 c) shows the values of $\tau(q)$ for $k_x = 0.02\pi$ and $k_x = 0.2\pi$, for several values of quasi-disorder strength λ for the size interval L_1. Unlike the previous case with Anderson disorder, we see that the results differ for each k_x, and that for some values of disorder strength $\tau(q)$ follows the line $q-1$ closely until some value of q where the behaviour suddenly changes. In 14 d) we show, as before, values of $\tau(q)$ fitted for the considered size intervals L_1, L_2, L_3 and L_4. For lower values of q, τ remains at the values defined by the equation $\tau(q) = D(q)(q-1)$ with $D(q) = 1$. However, at higher values of q, this behaviour changes. Contrary to the case in figure 14 b), there is no clear tendency of $\tau(q)$ at increased system sizes, and the behaviour also depends on the value of q. This deviation from the $D(q) = 1$ line is verified as soon as disorder is introduced, and suggests the system is in a multifractal regime. From inspection of the values of $\tau(q)$ at larger system sizes, we identify a transition to a single-fractal phase around $\lambda \in [2.0, 2, 1]$.

VI. CONCLUSIONS

In this work we studied a model of a two-dimensional topological superconductor with a magnetic field, and introduced disorder and quasi-disorder in the system.

The system was first studied on a real space approach, and under a parallel magnetic field. We discussed the case where either Anderson disorder or Aubry-André disorder is added to the edges. While the IPR of the bulk states remains nearly constant, the edge states significantly localize, although with a different behaviour for Anderson or Aubry-André disorder: in the first case, the IPR grows continuously and in the second it shows a threshold behaviour.

We then studied the cases of bulk disorder, with three different spatial configurations: Anderson disorder, Anderson disorder uniform in x and Aubry-André disorder, modulated in the y direction uniform in x. The response of the system to the types of disorder is qualitatively different. We observed an exponential-like behaviour of the IPR for Anderson disorder, a linear behaviour for Anderson disorder uniform in x, and a threshold behaviour for Aubry-André disorder with two different regions, separated at around $\lambda = 2$.

The real space system was also studied under a perpendicular magnetic field with Anderson and Aubry-André disorder uniform in the x direction. The response of the topological phases of the system differ to the introduced types of disorder, and quasi-disorder induces topological phases in new regions of B_z, characterized by integer values of the Chern number C. From a scaling analysis of the critical points we concluded that the obtained phase

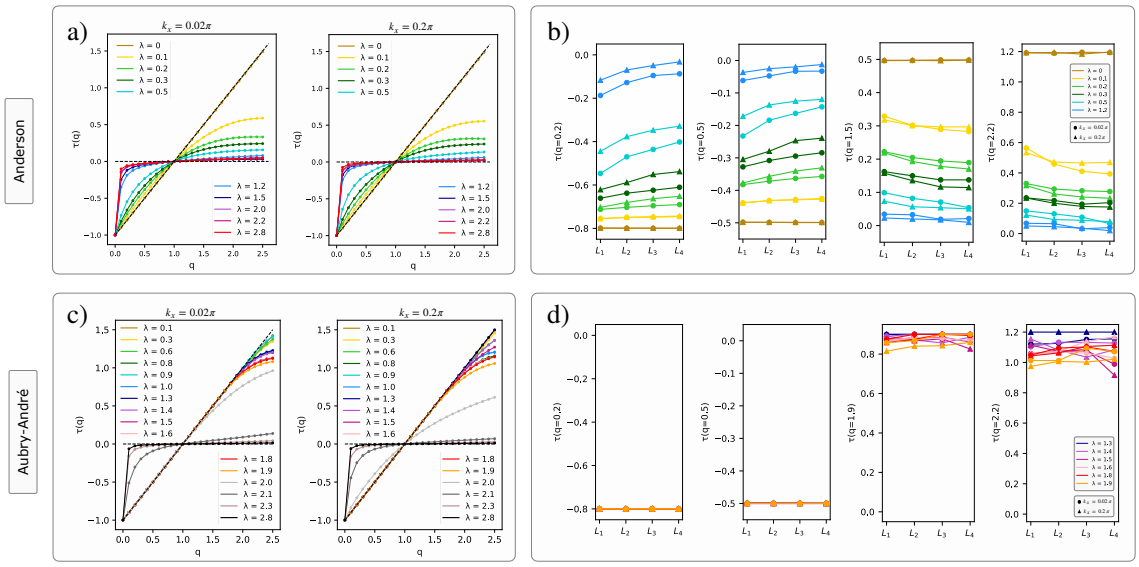

Figure 14. a) Results of τ vs. q, for several values of Anderson disorder strength, λ, for $k_x = 0.02\pi$ and $k_x = 0.2\pi$. b) Values of τ at different values of q and Anderson disorder strength λ, for $k_x = 0.02\pi$ and $k_x = 0.2\pi$. c) Results of τ vs. q, for several values of quasi-periodic disorder strength, λ, for $k_x = 0.02\pi$ and $k_x = 0.2\pi$. d) Values of τ at different values of q and quasi-disorder strength λ, for $k_x = 0.02\pi$ and $k_x = 0.2\pi$ In all cases, the IPR is averaged for the states within the energy range $E \in [0.05, 1]$.

diagrams should apply to bigger systems. For some low values of B_z we also found that x-periodic Anderson disorder induces some small regions of topology, in a region of magnetic field for which, in the clean system, $C = 0$ and $I(k_y) \neq 0$. In the same regions, new topological regions appear for added quasi-disorder. These observed phenomena were hypothesized to be related to the invariant $I(k_y)$.

We also studied the system in a mixed (k_x, y) space with an applied parallel magnetic field. We obtained that the flat bands are characterized by a π-quantized Berry phase in the clean system. From the definition of winding number $\mathcal{W}$ we also obtained the expressions for the topological gapless regions of the superconductor.

The introduction of quasi-disorder was shown to induce gapless phases. For the p-wave system this leads to new regimes with Majorana flat bands. We then concluded that the quasi-disorder induced MFBs also have a quantized Berry phase of π. For the noncentrosymmetric superconductor with added s-wave superconducting pairing and spin-orbit coupling, we found that new regimes with unidirectional Majorana edge states appear.

We identified and studied two topological transitions. The values of the dynamical critical exponents and correlation length critical exponents were obtained from a scaling analysis of the density of states, and our results put the transitions in a novel universality class.

Finally, we investigated the fractal nature of the wavefunctions. From the behaviour of $\tau(q)$ as the thermodynamic limit is approached, we concluded that the introduction of quasi-disorder induces multifractality in the system, and that Anderson disorder will drive the system to a localized, single-fractal phase (in the thermodynamic limit).

[1] C. Beenakker, Annual Review of Condensed Matter Physics **4**, 113 (2013).
[2] M. Z. Hasan and C. L. Kane, Reviews of Modern Physics **82**, 3045 (2010).
[3] X.-L. Qi and S.-C. Zhang, Reviews of Modern Physics **83**, 1057 (2011).
[4] M. Sato and S. Fujimoto, Physical Review B **79** (2009).
[5] C. L. M. Wong, J. Liu, K. T. Law, and P. A. Lee, Physical Review B **88** (2013).
[6] S. Aubry and G. André, Ann. Israel Phys. Soc **3**, 18 (1980).
[7] X. Wen and A. Zee, Nuclear Physics B **316**, 641 (1989).
[8] Y.-F. Zhang, Y.-Y. Yang, Y. Ju, L. Sheng, R. Shen, D.-N. Sheng, and D.-Y. Xing, Chinese Physics B **22**, 117312 (2013).
[9] N. Sedlmayr, J. M. Aguiar-Hualde, and C. Bena, Physical Review B **91** (2015), 10.1103/physrevb.91.115415.
[10] K. Kobayashi, T. Ohtsuki, K.-I. Imura, and I. F. Herbut, Physical Review Letters **112** (2014), 10.1103/physrevlett.112.016402.
[11] F. Wegner, Zeitschrift für Physik B Condensed Matter and Quanta **36**, 209–214 (1980).
[12] F. Evers and A. D. Mirlin, Reviews of Modern Physics **80**, 1355 (2008).